Polarimetric Scanning Radiometer C- and X-Band Microwave Observations During SMEX03

Thomas J. Jackson, *Fellow, IEEE*, Rajat Bindlish, *Member, IEEE*, Albin J. Gasiewski, *Fellow, IEEE*, Boba Stankov, Marian Klein, Eni G. Njoku, *Fellow, IEEE*, David Bosch, Tommy L. Coleman, Charles A. Laymon, *Member, IEEE*, and Patrick Starks

***Abstract*—Soil Moisture Experiment 2003 (SMEX03) was the second in a series of field campaigns using the National Oceanic and Atmospheric Administration Polarimetric Scanning Radiometer (PSR/CX) designed to validate brightness temperature (T_B) data and soil moisture retrieval algorithms for the Advanced Microwave Scanning Radiometer (AMSR-E) for the Earth Observing System on the Aqua satellite. Objectives related to the PSR/CX during SMEX03 included: calibration and validation of AMSR-E T_B observations over different climate/vegetation regions of the U.S. [Alabama (AL), Georgia (GA), Oklahoma (OK)], identification of possible areas of radio-frequency interference (RFI), comparison of X-band observations from Tropical Rainfall Measurement Mission Microwave Imager (TMI), AMSR-E, and PSR/CX, and exploring the potential of soil moisture retrieval algorithms using C- and X-band imagery in diverse landscapes. In the current investigation, more than 100 flightlines of PSR/CX data were extensively processed to produce gridded T_B products for the four study regions. Due to the lack of significant rainfall in OK, generally dry soil moisture conditions were observed. Observations obtained over AL include a wide range of soil moisture and vegetation conditions. Results from the AL site clearly showed a lack of sensitivity to rainfall/soil moisture under forest canopy cover. Quantitative comparisons made with the TMI validated that both the PSR/CX and AMSR-E X-band channels were well calibrated. Spectral analyses indicated that the PSR/CX observations at C-band also are reasonable. As expected, there were varying degrees of RFI in the AMSR-E C-band data for the study sites that will prevent further soil moisture analysis using these data. X-band comparisons of the PSR/CX high-resolution and AMSR-E and TMI low-resolution data indicated a linear scaling for the range of conditions studied in SMEX03. These results will form the basis for further soil moisture investigations.**

***Index Terms*—Advanced Microwave Scanning Radiometer (AMSR-E), passive microwave, soil moisture, validation.**

Manuscript received October 19, 2004; revised February 9, 2005. This work was supported in part by the National Aeronautics and Space Administration Earth Observing System AMSR-E Instrument Science Program, in part by the NASA Terrestrial Hydrology Program, in part by the Japan Aerospace Exploration Agency Advanced Microwave Scanning Radiometer Science Program, and in part by the National Oceanic and Atmospheric Administration Office of Oceanic and Atmospheric Research.

T. J. Jackson is with the Hydrology and Remote Sensing Laboratory, Agricultural Research Service, U.S. Department of Agrilcuture, Beltsville, MD 20705 USA (e-mail: tjackson@hydrolab.arsusda.gov).

R. Bindlish is with the Science Systems and Applications, Inc., Lanham, MD 20706 USA and also with the Hydrology and Remote Sensing Laboratory, Agricultural Research Service, U.S. Department of Agrilcuture, Beltsville, MD 20705 USA.

A. J. Gasiewski, B. Stankov, and M. Klein are with Environmental Technology Laboratory, National Oceanic and Atmospheric Administration, Boulder, CO 80305 USA.

E. G. Njoku is with the Jet Propulsion Laboratory, Pasadena, CA 91109 USA.

D. Bosch is with the Southeast Watershed Research Center, Agricultural Research Service, U.S. Department of Agrilcuture, Tifton, GA 31794 USA.

T. L. Coleman is with the Hydrology, Soil Climatology, and Remote Sensing Research Center, Alabama A&M University, Normal, AL 35762 USA.

C. A. Laymon is with the Global Hydrology and Climate Center, Huntsville, AL 35805 USA.

P. Starks is with the Grazinglands Research Laboratory, Agricultural Research Service, U.S. Department of Agrilcuture, El Reno, OK 73036 USA.

Digital Object Identifier 10.1109/TGRS.2005.857625

I. Introduction

GLOBAL remote sensing of soil moisture has been a major research goal for more than two decades. Low frequencies are preferable for soil moisture retrieval since perturbing factors such as vegetation are less significant. Recent advances in science and technology have resulted in space agency commitments to L-band (1.4 GHz) missions within the next five years [1], [2]. At present, there are several new satellite sensors operating at somewhat higher frequencies than L-band that show promise for soil moisture mapping under some conditions. The Advanced Microwave Scanning Radiometer (AMSR-E) provided by Japan onboard the National Aeronautics and Space Administration (NASA) Earth Observing System (EOS) Aqua satellite is one such sensor capable of retrieving soil moisture using microwave channels at 6.9 and 10.7 GHz. Aqua was launched in May 2002 and will provide a soil moisture product based on AMSR-E data in regions with low levels of vegetation [3]. Other related satellites are the Advanced Earth Observing Satellite 2 (ADEOS-II) AMSR, which has ceased operations, and the Coriolis WindSat.

Validation of the soil moisture products, as well as the brightness temperatures over land, from AMSR-E and the other satellite instruments is a critical issue and one that is difficult to address. The coarse spatial scale of these passive microwave instruments (40–75 km) and the high temporal and spatial variability of the soil moisture fields make extensive sampling and replication difficult and costly. A series of field experiments [Soil Moisture Experiment (SMEX)] were developed to address these needs using a combination of ground and aircraft observations. Each experiment focuses on a different set of climate and vegetation regimes but maintains, to the degree it is possible, a standard set of validation data. The National Oceanic and Atmospheric Administration (NOAA) Polarimetric Scanning Radiometer (PSR/CX) has been a key component of the experiments. It collects high spatial resolution data ($\sim$3 km) at the lower AMSR-E frequencies.

Here, the brightness temperature (T_B) results obtained by the PSR/CX during SMEX03 are analyzed. SMEX03 was conducted over sites in Oklahoma, Georgia, and Alabama during the summer of 2003. Aircraft data were processed to generate a series of calibrated, georegistered, and temporally normalized T_B products. Future investigations will focus on site-specific studies of soil moisture. Analyses included the PSR/CX T_B responses associated with general landscape features resulting from land cover and precipitation. In addition, data from the PRS/CX, AMSR-E, and Tropical Rainfall Measurement Mission (TRMM) Microwave Imager (TMI) sensors were compared to assess scaling, radio-frequency interference (RFI), and validation of AMSR-E T_B products. The passive microwave aircraft program to support AMSR-E algorithm development and validation was one of the most important components of SMEX03. The aircraft measurements provide a valuable link between the ground observations and the satellite measurements.

II. SMEX03 Description

Early soil moisture mapping experiments, such as the Washita92, Southern Great Plains (SGP97), and SGP99 experiments, were conducted over areas with minimal levels of vegetation water content ($< 2\text{kg} \cdot \text{m}^{-2}$) using low-frequency aircraft sensors. In SGP99, the PSR/C (an earlier version of the PSR/CX) was used with a soil moisture algorithm to map and assess retrievals across a wide range of soil moisture conditions under low to moderate vegetation [4]. SMEX02 was designed to extend the algorithm to areas with moderate to high vegetation water content conditions (4–8 $\text{kg} \cdot \text{m}^{-2}$). PSR/CX and AMSR-E data were collected in this campaign; however, problems with the early AMSR-E calibration and RFI in the region limited the analyses [5].

SMEX03 was designed to include the enhancement of the validation database for AMSR-E by including well-known study areas as well as additional climate/vegetation regimes. The field campaign took place during the summer of 2003. It involved four separate ground sampling regions; one near Huntsville, Alabama (AL), another near Tifton, Georgia (GA), and two previously studied regions in Oklahoma [Oklahoma North (ON) and Oklahoma South (OS)]. Each of these was at least 50 km $\times$ 75 km in size and corresponded to six, eight, or ten EASE-Grid cells. EASE-Grid is a regularly spaced mapping in cylindrical equal area projection [6]. The C-band AMSR-E footprint data (level 2A) with a resolution of approximately 60 km and a sampling resolution on the average of 10 km along with the geophysical ancillary data are mapped to an EASE-Grid with 25-km resolution. AMSR-E soil moisture retrievals are made using the EASE-Grid product. Corner coordinates of these regions are listed in Table I. Within each of these regions, ground-based soil moisture sampling was conducted at a minimum of 36 geographically distributed points. Ground sampling included gravimetric soil moisture measurements at a depth of 1 and 6 cm and dielectric probe measurements of the top 6 cm, soil temperatures, surface roughness, and vegetation parameters. Data collection, both aircraft and ground, was timed to coincide with a 3-h window centered on the Aqua equatorial overpass time of 13:30 LST. A brief description of the characteristics of each region follows.

Two different regional areas were mapped and sampled in Oklahoma, an area dominated by grasslands in the south (OS) and an area dominated by winter wheat in the north (ON). OS consisted of eight EASE-Grid cells, and ON had six. The overall character of the Oklahoma region is illustrated in Fig. 1, which is a false-color composite image created from a Landsat Thematic Mapper (TM) dataset collected on July 10, 2003. This image is a combination of bands 2, 3, and 4 as the blue, green, and red channels. Red areas in the image indicate vegetation. Whites and blues indicate bare soil and dormant or senescent vegetation. The ON region has very little vegetation cover during the summer because winter wheat is either senescent or harvested. Fig. 1 clearly illustrates the very different vegetation cover conditions of the two regions.

TABLE I
Locations of the SMEX03 Regional Study Sites

Region	Upper Left	Lower Right
Alabama (AL)	35.194 N 87.087 W	34.668 N 85.770 W
Georgia (GA)	31.803 N 83.971 W	30.961 N 83.364 W
Oklahoma South (OS)	35.422 N 98.342 W	34.443 N 97.700 W
Oklahoma North (ON)	36.871 N 98.047 W	36.107 N 97.418 W
Amazon forest	5.0 S 72.0 W	10.0 S 58.0 W
Sahara desert	22. 0 N 22.0 E	28.0 N 29.0 E
Mongolia	45.8 N 106.1 E	46.8 N 107.5 E

The OS region has been extensively studied in previous remote sensing experiments including SGP97 and SGP99 [4], and includes the Little Washita (LW) watershed. An *in situ* soil moisture network, as well as meteorological data, is available in this region. The ON region was also a part of SGP97 and SGP99. Both regions fall in a U.S. Department of Energy study area providing a wide range of data including soil moisture and rainfall. In addition, the Oklahoma Mesonet is distributed throughout the state and also provides a variety of meteorological observations including soil moisture.

Fig. 2 is a portion of a Landsat TM image of the Little River Georgia (GA) region consisting of eight EASE-Grid cells. This figure from July 20, 2003 illustrates the general vegetation conditions that were encountered in SMEX03. There is considerable forest, primarily pines in the uplands and along field edges, as well as some hardwoods in the stream bottoms. Forested areas are typically dark red in Fig. 2. The dominant crop types are peanuts and cotton. At the time of this particular Landsat observation, the crops were mature with a full canopy resulting in red tones. However, during the field campaign in GA, late June, both crops had partial canopy cover.

The Alabama (AL) study area spans the Alabama–Tennessee border in the Tennessee River Valley. Unlike all the other study regions in SMEX03, this study area was oriented east-west and consisted of ten EASE-Grid cells. Significant relief characterizes the eastern third of the study area. The remaining part of the study area has smooth or gently rolling terrain. Fig. 3 (a multiple date composite of Landsat TM images) illustrates the vegetation levels encountered in SMEX03. It should be noted that this image was obtained slightly earlier in the season and a few years prior to the SMEX03 field campaign and exhibits more bare soil than was encountered during the field campaign.

Most of the AL region consists of small and medium-sized farms. Agricultural land (pasture and cultivated land) accounts for about 40% of land use. Pasture accounts for about 72% of all agricultural land throughout the study area. Cultivated land

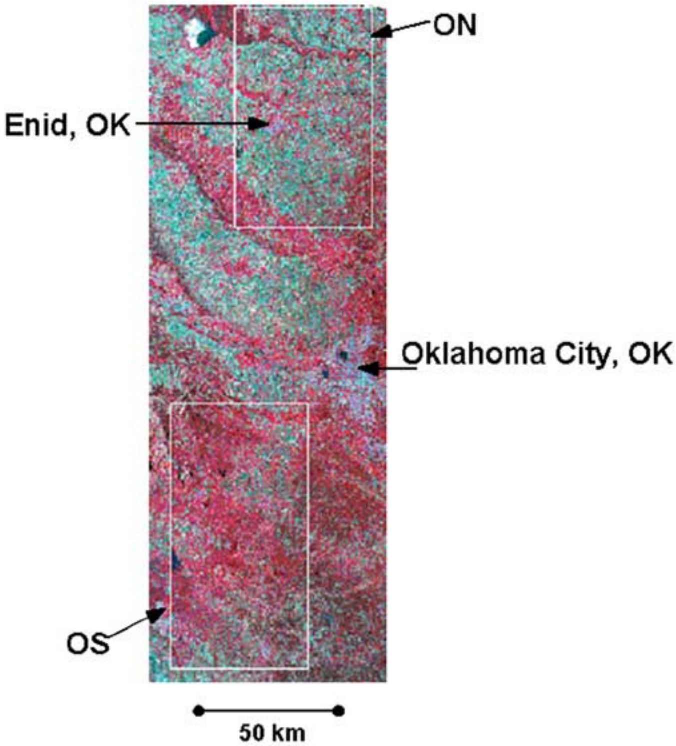

Fig. 1. Landsat TM false-color composite image (red = band 4, green = band 3, and blue = band 2) of the OS and ON regions. Image was acquired on July 10, 2003.

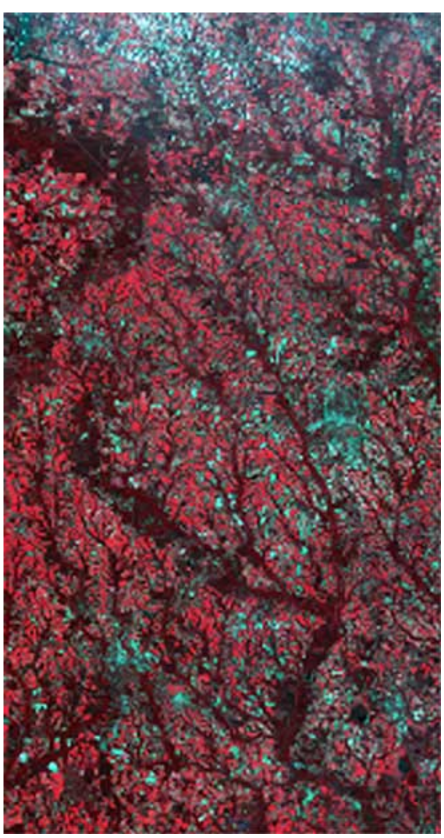

Fig. 2. Landsat TM false-color composite image (red = band 4, green = band 3, and blue = band 2) of the GA region. Image was acquired on July 20, 2003.

generally is located in the central and southwestern part of the study area, where relief is lowest. Crops are predominantly corn, soybeans, and cotton.

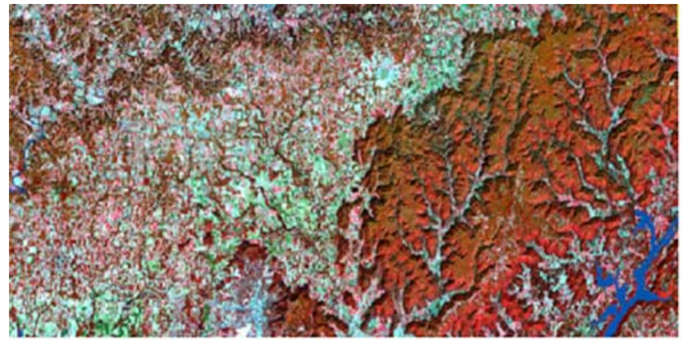

Fig. 3. Landsat TM false-color composite image (red = band 4, green = band 3, and blue = band 2) of the AL region. This is a composite from two images acquired on May 14 and April 19, 2000.

The amount of forested land ranges from about 27% in the western part to 68% in the eastern part of the study region where topographic relief is greatest (the dark red area in the right-hand portion of Fig. 3). The plateau and remnant "mountains" support a mixed oak-pine forest. Shortleaf pine, loblolly pine, sweetgum, yellow-poplar, red oaks, and white oaks are the major overstory species. Dogwood and redbud are major midstory species. Japanese honeysuckle, greenbrier, low panicums, bluestems, and native lespedezas are understory species.

III. Advanced Microwave Scanning Radiometer

Full details on AMSR-E and specifics on the soil moisture algorithm can be found in [3]. This instrument was developed by the Japanese Aerospace Exploration Agency (JAXA) and launched by NASA on the Aqua platform on May 4, 2002. AMSR-E makes dual-polarized passive microwave measurements at six frequencies: 6.9, 10.7, 18.7, 23.8, 36.5, and 89 GHz. The orbit is Sun-synchronous with equator crossings at 0130 and 1330 local solar time (LST).

The C- (6.9 GHz) and X-band (10.7 GHz) observations have potential for soil moisture estimation. Atmospheric effects at these frequencies are minimal, and it is possible to partially filter the effects of vegetation and surface roughness on the brightness temperature observations through relatively simple radiative transfer modeling. AMSR-E observations are available globally with a relatively short (2–3 day) repeat time and will form the basis for the first globally available daily soil moisture product [3]. Standard soil moisture products are a goal of both the NASA Aqua AMSR-E science team [3] and the Japanese ADEOS-II AMSR program [7].

It is hoped that the availability of these products will spawn new applications for remotely sensed soil moisture. However, hopes for AMSR-E soil moisture products have been tempered somewhat by the discovery that microwave measurements at C-band frequencies are contaminated with anthropogenic RFI [8]. The AMSR-E C-band radiometer makes observations with a central frequency of 6.925 GHz (350-MHz bandwidth) that is shared with fixed and mobile communication services and is subject to RFI contamination—particularly near large urban areas [3] and [9]. Some RFI has been reported in other AMSR-E channels [9].

In addition to RFI, there were problems with the very early versions of the C-band channel data related to the calibration [9]. It was found that low brightness temperatures were correct but higher values (typical of land targets) were overestimated by approximately 7 K for both H- and V-polarization. In September of 2003, the NASA AMSR-E program implemented a correction for this in their Level 2A dataset that utilizes a nonlinear calibration. This is called version B0 data. It should be noted that data produced by JAXA will not include this correction until 2005. The version of the AMSR-E data employed in the current investigation (B0) was obtained from the National Snow and Ice Data Center (http://nsidc.org/data/ae_l2a.html) on November 23, 2003.

IV. Polarimetric Scanning Radiometer

The PSR is an airborne microwave imaging radiometer operated by the NOAA Environmental Technology Laboratory [10] for the purpose of obtaining polarimetric microwave emission of the Earth's oceans, land, ice, clouds, and precipitation. It has been successfully used in several major experiments including SGP99 [4] and SMEX02 [5].

The PSR/CX scanhead houses two thermally stabilized polarimetric radiometers that share a common dual-band lens/feedhorn antenna. Each radiometer has four subbands that provide sensitivity to both vertical and horizontal polarization, along with an analog correlator that provides sensitivity to the third and fourth Stokes parameters at each of the two primary bands. The radiometers use internal noise diodes for rapid precalibration, along with external views of hot and ambient blackbody targets and cold space to provide absolute radio thermal calibration.

The PSR/CX radiometers are scanned in a conical mode using a gimbal drive mechanism (the PSR "positioner"). The positioner rotates the scanhead as fast as one rotation in $\sim$2.7 s. This rotation rate along with an 18-ms sample period provides near-Nyquist sampling of the scene below the aircraft at lower altitudes, and Nyquist sampling at higher altitudes ($>$2000 m). The sensitivity of the radiometers is better than 1 K for 18-ms integration time at most of the PSR/CX subbands.

The PSR/CX is housed within a gimbal-mounted scanhead drum. The scanhead drum is rotatable by the gimbal positioner so that the radiometers can view any angle within $\sim$ 70° elevation of nadir at any azimuthal angle, as well as external hot and ambient calibration targets. The configuration thus supports conical, cross-track, along-track, fixed-angle stare, and spotlight scan modes. Conical scanning at 55° incidence from nadir was used in SMEX03.

A network of precision clocks within the scanhead and controlling computers provides position/sample synchronization to better than one millisecond. An aircraft inertial navigation unit (INU) provided roll and pitch information at $\sim$10-ms intervals. These data were later used to correct the observed imagery for minor aircraft attitudinal variations.

The PSR/CX system provided simultaneous four-Stokes' vector measurements within four adjacent frequency subbands in both C- and X-bands (Table II). The multiband capability of PSR/CX allows the use of using frequency agile radiometry for observations over interference prone regions [11]. The primary lens/feedhorn antenna is located adjacent to a coboresighted video camera and longwave (10 μm) infrared sensor.

Calibration of all radiometers was performed in-flight using standard (unpolarized) hot and cold blackbody targets. The targets consist of an array of canted pyramidal iron-epoxy absorbing wedges organized in a two-faced L-shaped configuration. The pyramids are canted at an angle of 45° so as to provide maximum absorption in the direction of PSR/CX lens antennas. The absorbing pyramids overlie a thermally conducting substrate of aluminum pyramids so that the physical temperature of the entire structure remains homogeneous to within $\sim$1.5 K. In both hot and cold cases the effective emissivities of these targets were estimated using views of cold space obtained by rolling the aircraft steeply by 60° and pointing the radiometers to cold space at $\sim$ 40° above the horizon. The extremely cold observed brightness temperatures ($\sim$3.2 K) allowed the adjustment of the calibration target emission temperatures to achieve consistency across a wide range ($\sim$340 K) of T_B values.

During SMEX03, the PSR/CX scanhead was integrated into the NASA Wallops Flight Facility P-3B aircraft in the aft portion of the bomb bay. Spatial resolution and other features of the PSR/CX for the high-altitude lines are listed in Table III.

TABLE II
PSR/CX Channels for SMEX03

Frequency (GHz)	Frequency Band (GHz)	Polarizations	Beamwidth
6.00	5.82-6.15	v, h	10o
6.50	6.32-6.65	v, h	10o
6.92	6.75-7.10*	v, h, U, V	10o
7.32	7.15-7.50	v, h	10o
10.64	10.63-10.65	v, h	7o
10.69	10.68-10.70	v, h	7o
10.70	10.6-10.8*	v, h, U, V	7o
10.75	10.74-10.76	v, h	7o
Thermal	9.6-11.5 um	-	7o

*Indicates close to an AMSR-E channel.

TABLE III
PSR/CX Flightline and Mapping Specifications for SMEX03

Altitude (AGL) in m	7700
Number of f flight lines	4
Flight line length (km)	80
Flight line spacing (km)	11
Swath width (km)	19
Scan period (seconds)	3
Incidence angle (deg)	55
3-dB footprint resolution	3.0 km at 6 GHz 2.0 km at 10 GHz

V. Aircraft Data Collection and Processing

The NASA P-3B was deployed to Huntsville, AL from June 25 to July 2 to provide coverage of the AL and GA regions and was then moved to Oklahoma City to provide coverage of the OS and ON sites through July 18. High-altitude flights at 7700 m above ground level were conducted over all regions. Limited low-altitude flights were conducted over the Little

TABLE IV
SMEX03 P-3B SITE COVERAGE

Date	Sites	Satellite	Date	Sites	Satellite
June 25	AL, GA	Aqua	July 10	OS, ON	Aqua
June 27	AL	Aqua	July 11	ON	
June 29	AL, GA	Aqua	July 12	OS, ON	Aqua
June 30	AL, GA	Aqua	July 13	OS, ON	
July 2	AL, OS	Aqua	July 14	OS, ON	Aqua
July 3	OS, ON	Aqua	July 15	OS, ON	Aqua
July 5	OS, ON	Aqua	July 17	OS, ON	Aqua
July 7	OS, ON	Aqua			

Washita portion of OS. Table IV summarizes the flights conducted over each of the four regional sites. The P3-B flights were flown during midday in order to match the nominal Aqua overpass time of 1400 LST. Each flight was approximately 2 h in duration. Additional details can be found in the SMEX03 experiment plan http://hydrolab.arsusda.gov/smex03/ and in the data archive http://nsidc.org/data/amsr_validation/soil_moisture/smex03/.

PSR/CX raw data goes through several processing steps. Quality control, time synchronization, calibration, rasterization, and georegistration are considered preprocessing. Following this are RFI removal [10], adjusting for temporal variations inherent in mapping a large region with an aircraft sensor, and finally the data are resampled to a standard grid that facilitates multitemporal analysis and integration with ancillary data bases for algorithm applications. These three steps are described in the following sections.

In the course of processing the PSR/CX data from SMEX03, it was found that the X-band V-polarization data had inherent noise diode calibration problems that could not be corrected. Therefore, these data had to be deleted from analyses.

A. Removal of RFI and Subband Selection

An initial review of the PSR/CX data for all the C-band frequencies available indicated that anthropogenic RFI was present in all channels and both polarizations. RFI is manifested by higher than expected brightness temperatures, sometimes exceeding the nominal geophysical brightness temperatures by hundreds of Kelvins. In most cases the RFI was spatially localized, temporally consistent and often present in all channels simultaneously.

The purpose of using multiple subbands for each primary PSR/CX band is to provide a means of detecting anthropogenic radio-frequency interference. Such an interference detection and correction algorithm was successfully demonstrated using PSR data from SGP99 [4] and was applied to both C- and X-band in SMEX02 [5]. The algorithm works by comparing brightness temperatures in several nearby subbands through the use of a standard spectral model. This approach was used with the SMEX03 data. PSR/CX subbands could be used to identify the general location of the interference and to select the frequency band of least contamination. Relatively few occurrences of interference were noted at X-band.

Based upon a close examination of the RFI in the data, it was concluded that the 7.32- and 10.7-GHz bands were superior to the others. Therefore, all analyses used these channels. The resulting PSR/CX datasets should be nearly free of RFI.

B. Temporal Normalization

Collecting high-resolution radiometric data over a large region requires considerable aircraft flight time. For SMEX03, it took over an hour to complete a mapping session for a region on any given day. Both the surface emissivity and physical temperature can increase over the course of this interval. Other long-term drifts in instrument characteristics not accounted for in the calibration process could also contribute to brightness temperature variations over the flight period.

By design, the data from any given flight line partially overlapped the data from adjacent flight lines. To have the equivalent of an instantaneous snapshot of the region, it was necessary to normalize the observed imagery to a single time. It is assumed that no temporal correction was needed within a given flight line, but rather only from line to line. Next, the second of the four north–south lines on each day was used as a standard for that day. Following this, all data points that fell in the overlapping areas of the flight lines were identified and averaged by line. The average of this area for each line was compared to the same area for line 2 to determine a correction offset. This technique has been employed in previous aircraft missions [4] and [5].

C. Grid Resampling

The PSR/CX data consist of beam positions for sequential conical scans. Each beam position footprint is about 3 km in size. Due to sampling rates, the spacing between these footprints is 300 m, which results in over sampling. In addition, as described above, each line of data overlaps other lines. It is also desirable to produce datasets that can be integrated in further analyses. Therefore, all the footprint data were used in a kriging-based grid resampling procedure. The output grid selected was 800 m, which matched the nominal field scale in the regions as well as the resolution of other databases. Each channel of data was resampled independently.

VI. BRIGHTNESS TEMPERATURE IMAGE ANALYSES

In this section, the quality of the PSR/CX datasets collected in SMEX03 is assessed. Only the C-band H-polarization will be discussed because, based upon theory, this is expected to be the most responsive to soil moisture and least affected by vegetation. The other channels did behave in a similar manner and are included in the quantitative analyses in the next section. Patterns of T_B are interpreted in the context of measured precipitation and landscape features inferred from the previously presented Landsat imagery with supporting field observations. A limitation of the SMEX03 microwave observations, both satellite and aircraft, was the lack of a range in the observed soil moisture conditions. There was almost no rainfall during SMEX03 at the OS and ON sites resulting in constant dry soil conditions. There was significant rainfall over the AL region and limited rainfall over GA.

The observed sequence of gridded brightness temperature images for OS is shown in Fig. 4. The only rainfall that occurred

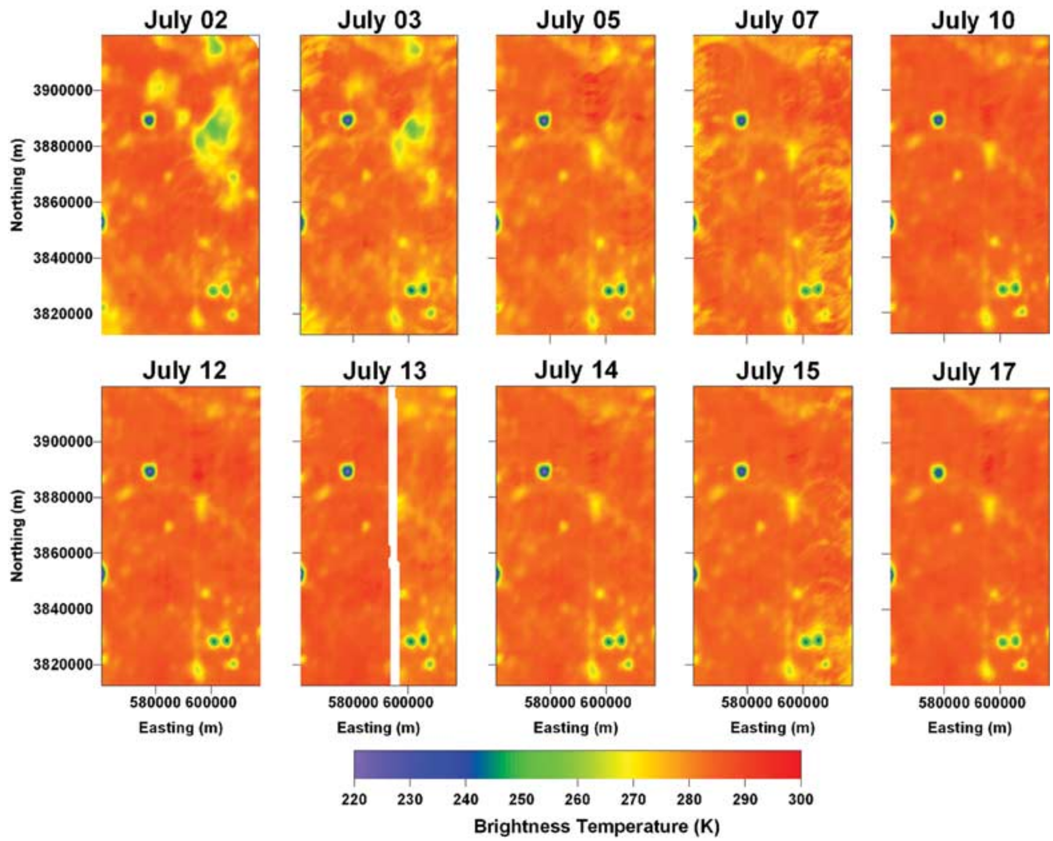

Fig. 4. PSR 7.32-GHz H-polarization brightness temperature images for the OS region.

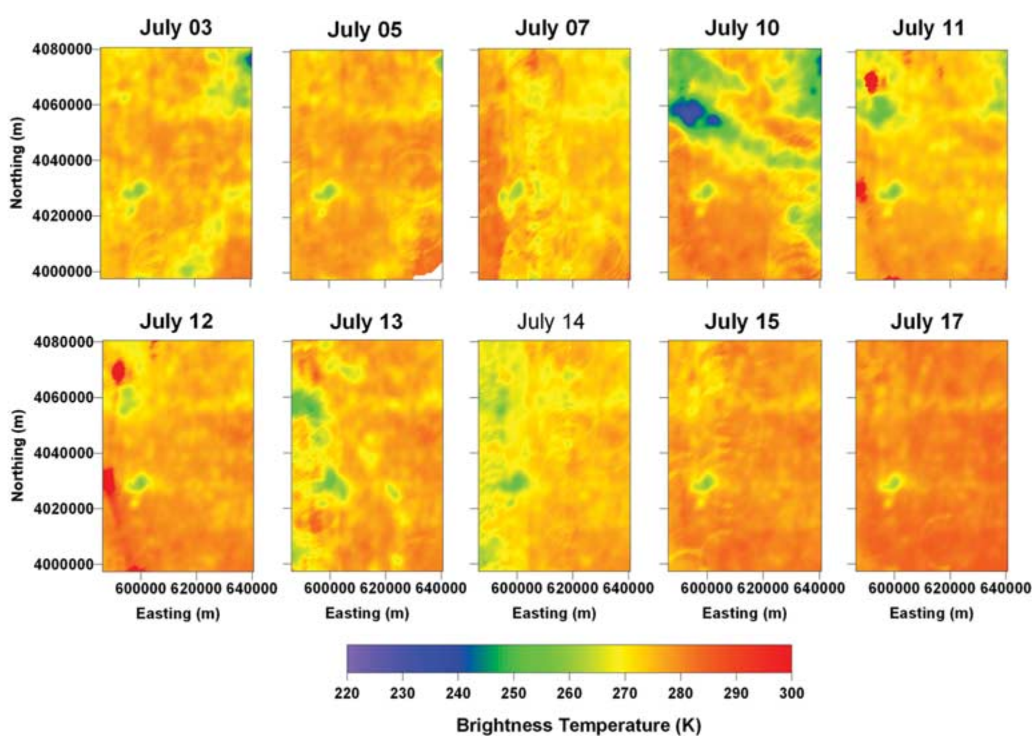

Fig. 5. PSR 7.32-GHz H-polarization brightness temperature images for the ON region.

in this region during the entire period was on July 1. This is reflected in the lower T_B values in the northeast portion of the image. This lower T_B area shrinks on July 3 and is nearly gone by July 5. The overall levels of T_B are remarkably consistent from day to day. The only significantly different features in the image sequence are a number of small water bodies in the region. Fig. 1 indicates rather uniform vegetation conditions in the OS region.

Fig. 5 is the sequence of images obtained for ON. Much the same precipitation conditions discussed for OS were encoun-

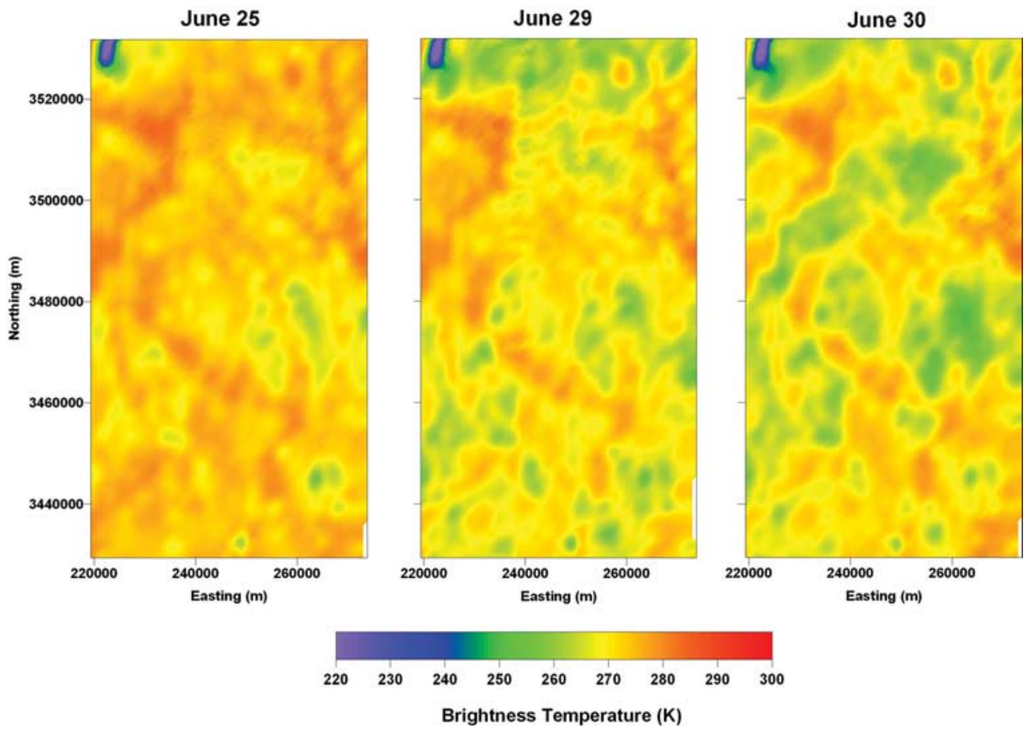

Fig. 6. PSR 7.32-GHz H-polarization brightness temperature images for the GA region.

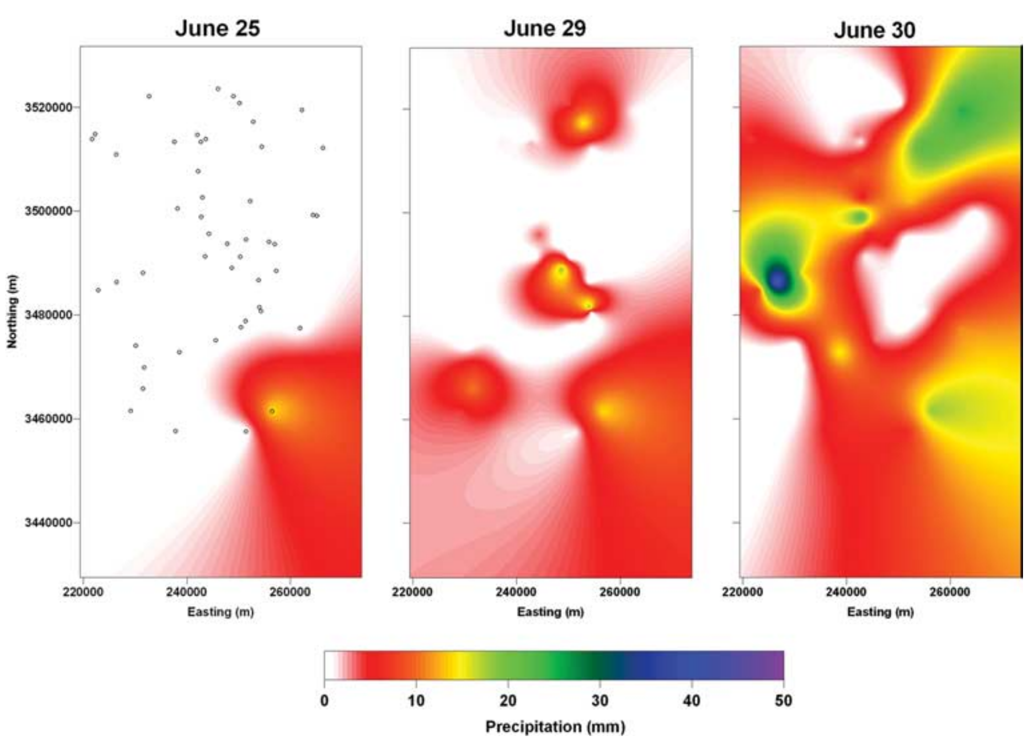

Fig. 7. Precipitation images for events during SMEX03 in the GA region.

tered in the ON region. In the ON region there was a single event prior to the July 10 flight that impacted a portion of the region. Much of the decrease in T_B associated with this event was gone in the data collected the next flight day. Two features of note in the image sequence are the city of Enid (also see Fig. 1) located in the northwest portion of the image (slightly lower values of T_B each day) and two small lakes near Oklahoma City (also see Fig. 1) in the southeast. Fig. 1 indicates fairly consistent land cover throughout the region. The overall levels of T_B are slightly lower in this region than in OS, which may reflect the overall lower amount of vegetation in ON.

Fig. 6 shows the three images obtained for the GA region. These images show interesting features as the result of precipitation and more spatially variable vegetation conditions than encountered in OS and ON. The last rainfall prior to the June 25 T_B image occurred on June 20. Therefore, high T_B values were ex-

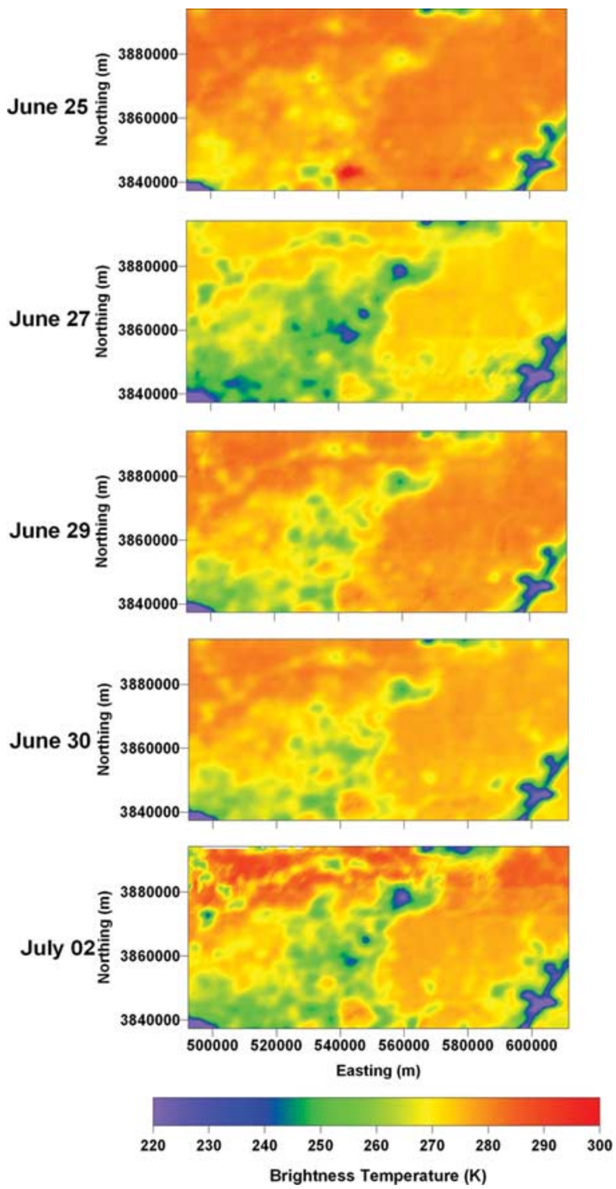

Fig. 8. PSR 7.32-GHz H-polarization brightness temperature images for the OS region.

pected. There are also patterns in this image that are the result of the vegetation cover. All of the darker red areas in Fig. 2, which are mostly forested, correspond to higher T_B values. There are a few areas with lower T_B values that are associated with the drainages.

Rainfall in the GA region was provided by cumulative gauges placed in fields used for soil moisture sampling. These locations are indicated in Fig. 7. Readings were made at the time of soil moisture sampling and corresponded to the rainfall in the 24 h prior to local noon, which was just prior to the aircraft data collection. Although this is a rather dense network the precision of this type of gauge is not high. These data were used in a kriging-based interpolation procedure to generate gridded images of the region. These images are intended only to illustrate patterns and are not used in any further quantitative analyses. Rain events occurred prior to the June 29 and June 30 flights. Interpolated images of the antecedent rainfall for these dates are shown in Fig. 7.

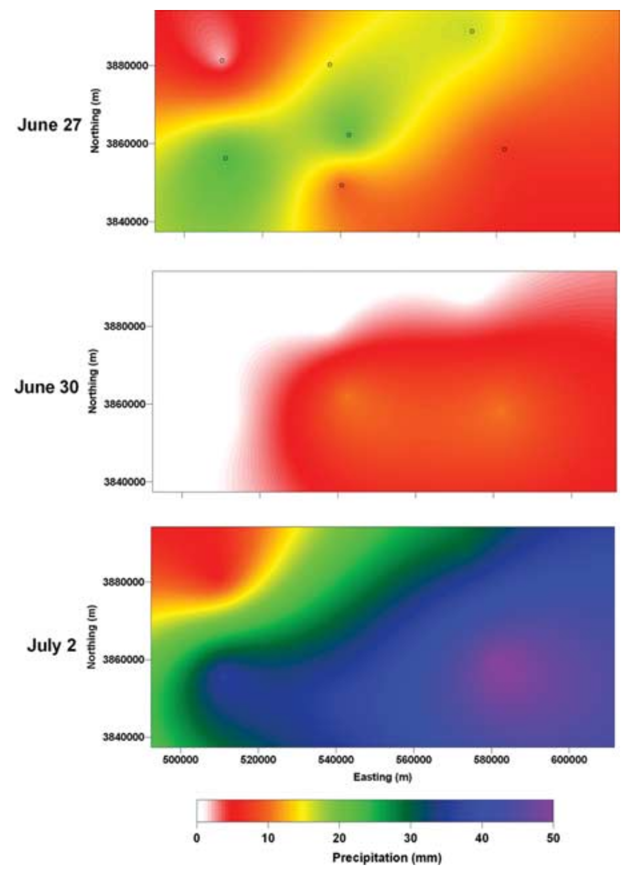

Fig. 9. Precipitation images for events during SMEX03 in the AL region.

The rainfall was light over most of the GA region prior to June 29. Comparing Figs. 6 and 7 for June 29 it is observed that there was very little change in T_B from the preceding dry day (June 25) over much of the region. Unfortunately the areas where there were changes in T_B corresponded to areas with fewer rain gauges. Therefore, it would be difficult to infer more information from this date without utilizing the actual soil moisture observations.

The rainfall image for June 30 (Fig. 7) shows that significant rain occurred in some areas of the GA region prior to the aircraft data collection on that date. Comparing the rainfall (Fig. 7), land cover (Fig. 2), and T_B values (Fig. 6) it appears that this amount of rain reduced T_B values over both the agricultural fields and portions of what were interpreted as forested areas from Fig. 2. As in the case of the June 29 observations, the highly variable rainfall and mixed land uses make it difficult to comment any further without soil moisture observations.

The data collected in AL are the most interesting and straight forward to interpret of all the SMEX03 datasets. The first thing to point out for the AL region is that there are three well-defined vegetation domains in Fig. 3. The northwest is mixed forest and pasture, the balance of the western half is cropland intermixed with pasture, and the eastern half is forest. In Fig. 8 there are consistent spatial features of the T_B values that are the result of these land cover variations. A river and reservoir are located on the eastern edge and southwest corner of the images (low T_B values).

For the AL analyses, ground data collected as part of a cooperative project between Alabama A&M University

Fig. 10. Photo of ground and canopy conditions within the AL forest area during SMEX03.

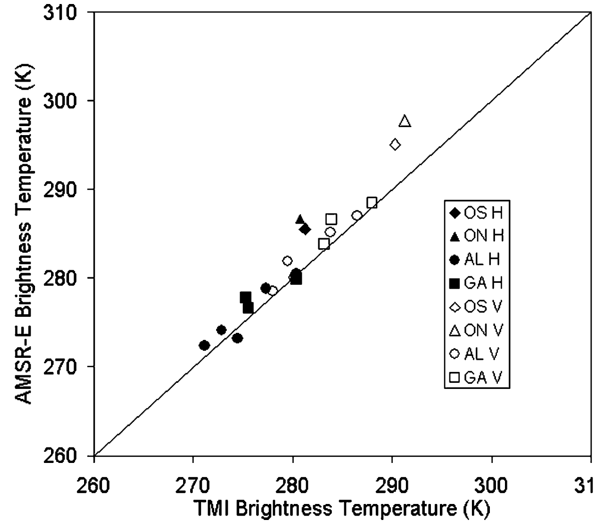

Fig. 11. Comparison of X-band brightness temperature data collected by TMI and AMSR-E X during SMEX03. The legend indicates the site and polarization.

and the USDA Soil Climate Analysis Network (SCAN) (http://www.wcc.nrcs.usda.gov/smst/smst.html) were used. There were a total of ten stations distributed in or near the AL region; the locations of those within the mapping region are shown in Fig. 9. Data are reported on an hourly basis. For each flight date, the cumulative rainfall from the previous flight, up to the time of the aircraft over flight, was computed. As in the case of the GA data, the point observations were used to produce the resampled grid images.

The June 25 T_B images shown in Fig. 8 are fairly uniform and represent dry conditions, since there had been no rain in the region for several days. Rainfall between the June 25 and 27 T_B images is shown in Fig. 9. From this figure, we observed that the rain was widespread but heaviest in the central portion of the image, which corresponded to the lowest vegetation levels. Therefore, in attempting to interpret the T_B image for June 27 it was not possible to separate the effects of lighter vegetation in the eastern portion from the increased vegetation levels associated with a forest canopy. An overall decrease of T_B values in the July 27 image is likely the result of decreased physical temperature since the rainfall occurred just a few hours before the flight. The next precipitation occurred on June 30 during the early morning on the day of the flight. As shown in Fig. 9, the rainfall was light and there was likely no precipitation in the western portion. In the T_B image sequence of Fig. 8 there is an increase between June 27 and 29 that was likely the result of drying. The June 29 and 30 images are very similar.

Between the flight on June 30 and that of July 2 there was extended and significant rainfall throughout the region (Fig. 9). Here, the eastern-forested portion received the most rainfall (over 5 cm). The central portion of the July 2 T_B image (Fig. 8), which was agriculture, exhibited a decrease in T_B values; however, no change in T_B was observed for the forested area between June 30 and July 2 even though there was significant antecedent rainfall. This result clearly demonstrates the lack of sensitivity to soil moisture changes when using a C-band sensor in this particular forested region. Fig. 10 illustrates the canopy/understory conditions in this forested region. These are not exceptionally dense forest canopy conditions. The canopy leaf water content was estimated to be approximately, 1.6 kg/m^2 (John Kimball, personal communication).

VII. Comparison of AMSR-E, TMI, and PSR Brightness Temperatures

One of the goals in SMEX03 was to contribute to the validation of the low-frequency brightness temperature products generated from Aqua AMSR-E over land. Since this analysis involves the PSR/CX data it also addresses an important science question; do the high-resolution aircraft T_B data ($\sim$3 km) scale directly to the coarse-resolution satellite observations ($\sim$50 km)? In this section, the results of a multiple-step analysis are presented that address these validation and scaling issues. First, TMI X-band observations are compared to similar PSR/CX and AMSR-E channels. Following this, the relationships between X- and C-band channels is examined. Finally, an evaluation of the PSR/CX and AMSR-E X- and C-band channels is presented.

All datasets for the four regional study areas that had concurrent observations of TMI and AMSR-E, TMI, and PSR/CX, or AMSR-E and PSR/CX were identified. It was noted earlier that for this investigation the definition of concurrent is within 1 h of each other. No attempt was made to temporally adjust any of the datasets. This resulted in a moderate number of samples for each combination but fewer for the TMI comparisons. This is due to the constantly changing time of observations of the TMI; only a few days had observations close enough to the AMSR-E observing time. It was also noted previously that the PSR/CX X-band V-polarization data were not considered to be reliable and was not analyzed here.

For each of the instruments being used, all footprints with centers that fell at least 10 km inside the study regions were averaged. This typically resulted in $>$50 for TMI, $>$27 for AMSR-E, and $>$160 000 for PSR/CX.

The starting point in this analysis is the stipulation that the TMI is a well-calibrated radiometer. This seems a reasonable assumption since TMI has been in operation for five years and many investigators have evaluated the data. Therefore, comparisons of the AMSR-E and PSR/CX X-band channels to the TMI data should indicate how well the same channels of these instruments were calibrated. Fig. 11 shows the TMI versus the AMSR-E data. The results indicate a nearly one-to-one correspondence between the two datasets for both H- and V-polarization. The bias for H-polarization was 0.6 K (AMSR-

TABLE V
STATISTICAL COMPARISON OF AIRCRAFT AND SATELLITE BRIGHTNESS TEMPERATURE DATASETS

Comparison	Bias (°K)	Standard Error of Estimate (°K)
X-band V Polarization (AMSR-E – TMI)	1.0	2.0
X-band H Polarization (AMSR-E – TMI)	0.6	2.1
X-band H Polarization (PSR/CX – TMI)	0.3	2.0
X-band H Polarization (PSR/CX - AMSR-E)	-1.0	2.7
AMSR-E H Polarization (X-band - C-band)	-0.2	1.8
PSR/CX H Polarization (X-band - C-band)	3.3	4.7

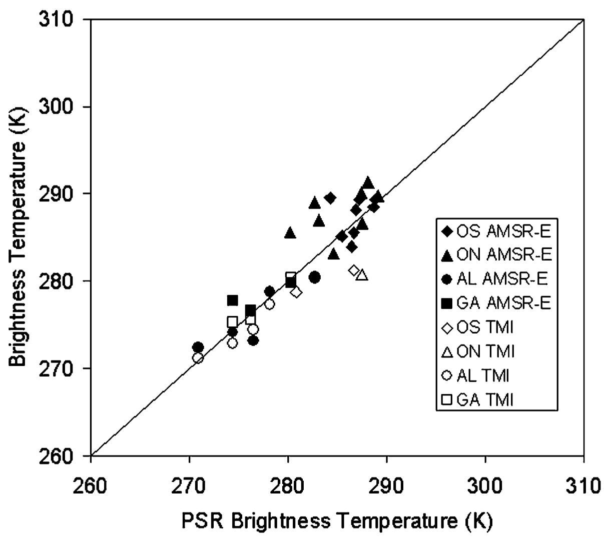

Fig. 12. Comparison of X-band H-polarization brightness temperature data collected by the PSR/CX with TMI and AMSR-E X data during SMEX03. The legend indicates the site and satellite source.

E—TMI) and the standard error of estimate (SEE) was 2.1 K. The SEE may be the result of several factors. The higher spatial resolution of the TMI will result in a somewhat smaller area being averaged since we are averaging all footprints that fall at least 10 km inside the study area boundaries. Temporal variation within the 1-h time window selected can also contribute. Other results are summarized in Table V. These results support the assumption that the AMSR-E X-band channels are well calibrated in the range of observed T_B.

The next comparison is between the PSR/CX X-band H-polarization data and the similar TMI and AMSR-E channels. This set of results is shown in Fig. 12. Generally unbiased relationships were observed (0.3 K for PSR—TMI and -1.0 K for PSR—AMSR-E). The scatter appears similar to that found in Fig. 11 (SEE value of 2.0 K for PSR—TMI). Statistics are summarized in Table V. Increased scatter (SEE) was anticipated due to the large difference in spatial scales of the aircraft and satellite observations. However, the SEE did not increase significantly. In addition, the results are unbiased. These results suggest that the scaling from higher resolution aircraft observations to coarser satellite measurements is close to linear for the range of conditions studied in SMEX03.

Evaluation of the C-band data from the PSR/CX and AMSR-E is not as straightforward as the X-band analysis since

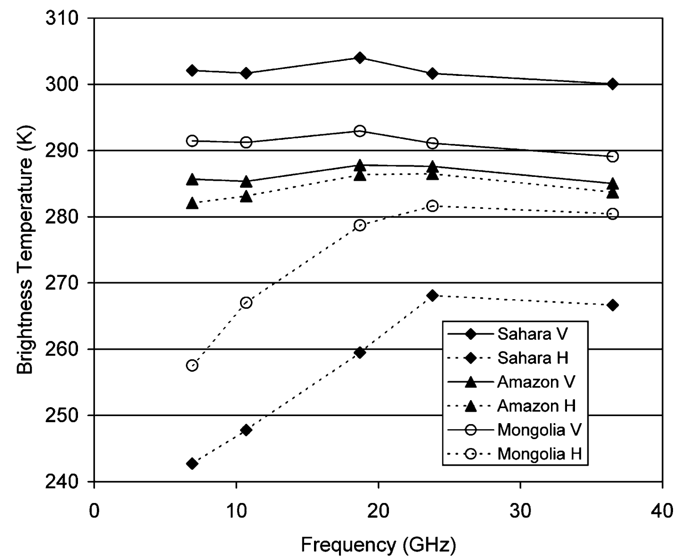

Fig. 13. Average brightness temperature as a function of frequency during the SMEX03 time period for homogeneous land sites.

the TMI data cannot be used as a reference and neither instrument has a validated calibration. The previous analyses did, however, establish the reliability of the X-band data. Therefore, we will attempt to use this as a reference and establish a link between X- and C-band. The basis of this is the spectral behavior (T_B as a function of frequency). From theory [9], [12], the emissivity of soil and vegetation should tend to increase as frequency increases. Over the AMSR-E frequency range the dielectric constant of soil and water exhibit small decreases, which could result in an increase in emissivity with frequency. Another soil related factor is that a shallower soil layer contributes to the measurement as frequency increases. Since the surface is typically drier than deeper layers, an increase in emissivity with frequency might be expected. Vegetation can increase emissivity as the result of increased masking of the soil surface. However, there is also the possibility that at higher frequencies the size of the vegetation components may contribute to increased scattering and lower values of T_B. Based upon these various considerations, it is anticipated that the X-band T_B values will be greater than the C-band values.

The spectral behavior described above can be examined using the observed T_B for specific types of land cover and the SMEX03 study sites. As noted in [9], when using T_B instead of emissivity, the atmospheric effects must be considered. These will tend to impact the frequencies higher than X-band. As a result, it is possible to observe decreases or increases at specific frequencies. Following the approach used in [9] we averaged the data for each site over a one-month period encompassing the SMEX03 study period. Only the ascending AMSR-E data were used.

As a first step in the spectral analysis we examined AMSR-E data for three regions of homogeneous land cover where the possibility of RFI contamination is low: the Amazon forest, the Sahara desert, and a grassland region in Mongolia. Corner coordinates of these sites are listed in Table I. Fig. 13 is a plot of AMSR-E T_B as a function of frequency. The absolute levels of T_B cannot be compared between sites because of the different temperature regimes. However, the patterns and differences between H- and V-polarization are relevant. For all sites

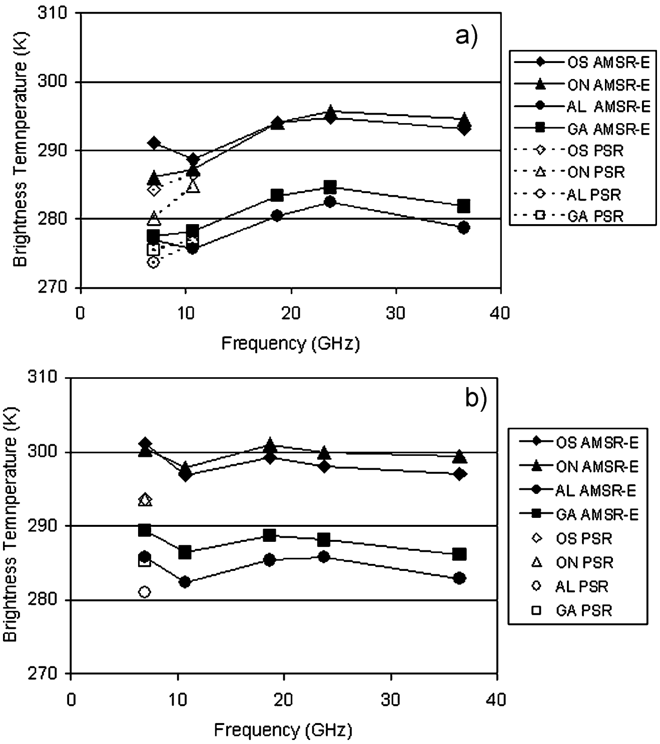

Fig. 14. Average brightness temperature as a function of frequency during the SMEX03 time period for the SMEX03 study sites. (a) H-polarization. (b) V-polarization.

the V-polarization T_B is nearly constant as a function of frequency. For H-polarization the T_B increases with frequency. The rate of change at the lower frequencies is a function of the amount of vegetation. For the Amazon, with the densest vegetation, the T_B is nearly constant over the AMSR-E frequency spectrum. The difference between the C-band V- and H-polarization observations over the Amazon is small due to the presence of vegetation (~3 K). This difference in C-band V- and H-polarization observations increases (~35 K) over Mongolia (sparse vegetation) and over the Sahara desert (~60 K). As the frequency increases the effect of vegetation and atmosphere increases, resulting in a decrease in the difference between V- and H-polarization values. In addition, we also examined each day of data on an individual basis to establish that average represented the daily trends.

Data for the SMEX03 sites are plotted in Fig. 14. The PSR/CX H-polarization data [Fig. 14(a)] exhibit the pattern that we expect to see based upon theory, an increase in T_B as frequency increases from C-to X-band. The PSR/CX results indicate that X-band T_B was 3.3 K higher than C-band. Fig. 14(a) and Table V summarize the results for H-polarization.

As noted previously, only the H-polarization could be used in this portion of the analysis since the X-band V-polarization had to be deleted. A comparison of the PSR/CX C-band H- and V-polarization indicated that V was larger than H by 10.6 K (ranging from 8.3 K in AL to 13.5 in ON). The difference between the V- and H band observations should be smaller over vegetated areas (AL was 50% forested), than the difference over sparse vegetation (ON was mostly harvested winter wheat). This relationship between the amount of vegetation and the difference in V- and H-polarization observations is also seen when comparing AMSR-E observations over the Amazon and Sahara regions. From theory and observations (Fig. 13), it is expected that the V-polarization T_B should be larger than the H-polarization value.

The AMSR-E data for the SMEX03 study sites do not exhibit the pattern that is expected from theory or the reference sites presented in Fig. 13. For H-polarization [Fig. 14(a)], all sites exhibited a decrease in T_B from C-to X-band. A review of the spatial and temporal patterns of AMSR-E C- and X-band T_B data from the study sites suggests that there was C-band RFI present at various levels in all sites. As described in [9], RFI will tend to increase the C-band T_B resulting in the patterns we observe in Fig. 14(a). ON and GA followed the expected trend, which suggests that these H-polarization data may not be as contaminated. It was also observed for V-polarization [Fig. 14(b)] that a decrease in T_B from C-to X-band occurred for all sites. Therefore, it appears that there are different issues involved in the H- and V-polarization data. This suggests that RFI may have polarization dependence.

The comparisons above indicate that the PSR/CX X-band H- and C-band H channels are accurately calibrated. AMSR-E X-band data is also considered to be accurate. However, RFI contamination in the AMSR-E C-band channels prevents use of the data in soil moisture retrieval at these sites.

VIII. Summary

Validation of the soil moisture products, as well as the brightness temperatures over land, from AMSR-E and the other satellite instruments is a critical issue and one that is difficult to address. The coarse spatial scale of these passive microwave instruments (40–75 km) and the high temporal and spatial variability of the soil moisture fields make extensive sampling and replication difficult and costly. A series of field experiments (Soil Moisture Experiment) were developed to address these needs using a combination of ground and aircraft observations.

Here, the brightness temperature results obtained by the PSR/CX during SMEX03 were analyzed. Data from four diverse regions were utilized. Aircraft data were processed to generate a series of calibrated, georegistered, and temporally normalized brightness temperature products. Analyses included the PSR/CX brightness temperatures responses associated with general landscape features resulting from land cover and precipitation. The value of the data collected in Oklahoma for this portion of the analysis was very limited due to a small range of observed moisture conditions. Data collected in Alabama included a wide range of antecedent rainfall conditions and diverse vegetation cover. Results indicated a lack of sensitivity to rainfall/soil moisture under the forest canopy conditions typical of the region at C-bands.

In addition, data from the PRS/CX, AMSR-E, and TMI sensors were compared to assess scaling, RFI, and validation of AMSR-E brightness temperatures products. These comparisons validated the AMSR-E and PSR/CX X-band H-polarization calibrations, which indicated linear scaling from the aircraft to satellite observations. PSR/CX C-band H-polarization data were also validated; however, there was RFI present in the AMSR-E C-band observations. The presence of RFI will eliminate these data from further analyses.

The results of the analyses conducted here have established the quality of both PSR/CX X- and C-band data and AMSR-E X-band data collected in SMEX03. With this knowledge, further soil moisture and geophysical interpretations can be performed with confidence.

ACKNOWLEDGMENT

The aircraft data are available from the National Snow and Ice Data Center at http://nsidc.org/data/amsr_validation/soil_moisture/smex03/.

REFERENCES

[1] Y. H. Kerr, P. Waldteufel, J. P. Wigneron, J. Font, and M. Berger, "Soil moisture retrieval from space: The Soil Moisture Ocean Salinity (SMOS) mission," *IEEE Trans. Geosci. Remote Sens.*, vol. 39, no. 8, pp. 1729–1735, Aug. 2001.

[2] D. Entekhabi, E. Njoku, P. Houser, M. Spencer, T. Doiron, J. Smith, R. Girard, S. Belair, W. Crow, T. Jackson, Y. Kerr, J. Kimball, R. Koster, K. Mcdonald, P. O'Neill, T. Pultz, S. Running, J. Shi, E. Wood, and J. Van Zyl, "An Earth system pathfinder for global mapping of soil moisture and land freeze/thaw: The Hydrosphere State (HYDROS) mission concept," *IEEE Trans. Geosci. Remote Sens.*, vol. 42, no. 10, pp. 2184–2195, Oct. 2004.

[3] E. G. Njoku, T. J. Jackson, V. Lakshmi, T. K. Chan, and S. V. Nghiem, "Soil moisture retrieval from AMSR-E," *IEEE Trans. Geosci. Remote Sens.*, vol. 41, no. 2, pp. 215–229, Feb. 2003.

[4] T. Jackson, A. Gasiewski, A. Oldak, M. Klein, E. Njoku, A. Yevgrafov, S. Christiani, and R. Bindlish, "Soil moisture retrieval using the C-band Polarimetric Scanning Radiometer during the Southern Great Plains 1999 experiment," *IEEE Trans. Geosci. Remote Sens.*, vol. 40, no. 10, pp. 2151–2161, Oct. 2002.

[5] R. Bindlish, T. J. Jackson, A. J. Gasiewski, M. Klein, and E. G. Njoku, "Soil moisture mapping and AMSR-E validation using the PSR in SMEX02," *Remote Sens. Environ.*, to be published.

[6] R. Armstrong, M. J. Brodzik, and A. Varani, "The NSIDC EASE-grid: Addressing the need for a common, flexible, mapping and gridding scheme," *Earth Syst. Monitor*, vol. 7, no. 4, 1997.

[7] T. Koike, E. G. Njoku, T. J. Jackson, and S. Paloscia, "Soil moisture algorithm development and validation for the ADEOS/AMSR," in *Proc. IGARSS*, Honolulu, HI, Jul. 24–28, 2000.

[8] L. Li, E. G. Njoku, E. Im, P. Chang, and K. St. Germain, "A preliminary survey of radio-frequency interference over the U.S. in Aqua AMSR-E data," *IEEE Trans. Geosci. Remote Sens.*, vol. 42, no. 2, pp. 380–390, Feb. 2004.

[9] E. G. Njoku, T. Chan, W. Crosson, and A. Limaye, "Evaluation of the AMSR-E data calibration over land," *Ital. J. Remote Sens.*, vol. 30/31, pp. 19–38, 2004.

[10] J. R. Piepmeier and A. J. Gasiewski, "High-resolution passive polarimetric microwave mapping of ocean surface wind vector fields," *IEEE Trans. Geosci. Remote Sens.*, vol. 39, no. 3, pp. 606–622, Mar. 2001.

[11] A. G. Gasiewski, M. Klein, A. Yevgrafov, and V. Leuskiy, "Interference mitigation in passive microwave radiometry," in *Proc. IGARSS*, vol. 3, Toronto, CA, Jun. 2002, pp. 1682–1684.

[12] N. C. Grody, "Surface identification using satellite microwave radiometers," *IEEE Trans. Geosci. Remote Sens.*, vol. 26, no. 6, pp. 850–859, Nov. 1988.

Thomas J. Jackson (A'86–SM'96–F'02) received the Ph.D. degree in civil engineering from the University of Maryland, College Park, in 1976.

He is currently a Hydrologist with the U.S. Department of Agriculture's Agricultural Research Service Hydrology and Remote Sensing Laboratory, Beltsville, MD. His research involves the application and development of remote sensing technology in hydrology and agriculture. His initial research with USDA extended his Ph.D. work on the use of visible/near-infrared satellite data for deriving land cover parameters used in hydrologic models. He has also investigated the use of an airborne laser profiler for measuring and monitoring soil erosion. The results of this research resulted in a paper "Airborne Laser Measurements of the Surface Topology of Simulated Concentrated Flow Gullies." His current research focuses on the use of passive microwave techniques in hydrology. These studies have ranged from small-scale controlled condition field experiments utilizing truck-mounted radiometers to large-scale multitemporal aircraft mapping. He is the Leader of a series of large-scale field experiments designed to extend high-resolution research to satellite scales. In conjunction with this, he is a Principal Investigator of studies involving SSM/I, TRMM, ADEOS-II, Aqua, Envisat, and ALOS.

Dr. Jackson received The Paper of the Year Award from the American Society of Agricultural Engineers for his paper "Airborne Laser Measurements of the Surface Topography of Simulated Concentrated Flow Gullies" in 1990, and the Prize Paper Award for his "Diurnal Observations of Surface Soil Moisture Using Passive Microwave Radiometers" at the International Geoscience and Remote Sensing Symposium in 1994. in 1999, he received the National Soceity of Professional Engineers 1999 Engineer of the Year Award for USDA ARS. In 2000, his work on aircraft mapping "Soil Moisture Mapping With Passive Microwave Imagery Data and Geostatistical Analysis" received the Remote Sensing and Hydrology 2000 Sympoisum Best Paper Award from the International Association of Hydrological Sciences. He is a Fellow of the American Geophysical Union and currently serves on the Administrative Committee of the IEEE Geoscience and Remote Sensing Society.

Rajat Bindlish (M'00) received the B.S. degree in civil engineering from the Indian Institute of Technology, Bombay, and the M.S. and Ph.D. degrees in civil engineering from The Pennsylvania State University, University Park, in 1993, 1996, and 2000, respectively.

He is currently with SSAI, Lanham, MD, working at the U.S. Department of Agriculture's Agricultural Research Service, Hydrology and Remote Sensing Laboratory, Beltsville, MD. His research interests involve the application of microwave remote sensing in hydrology. He is currently working on soil moisture estimation from microwave sensors and their subsequent application in land surface hydrology.

Albin J. Gasiewski (S'81–M'88–SM'95–F'02) received the B.S. and M.S. degrees in electrical engineering and the B.S. degree in mathematics, all from Case Western Reserve University, Cleveland, OH, in 1983, and the Ph.D. degree in electrical engineering and computer science from the Massachusetts Institute of Technology, Cambridge, in 1989.

From 1989 to 1997, he was Faculty Member within the School of Electrical and Computer Engineering, Georgia Institute of Technology (Georgia Tech), Atlanta. As an Associate Professor at Georgia Tech, he developed and taught courses on electromagnetics, remote sensing, instrumentation, and wave propagation theory. He is currently with the U.S. National Oceanic and Atmospheric Administration's (NOAA) Environmental Technology Laboratory (ETL) in Boulder, CO, where he is Acting Chief of the ETL Microwave Systems Development Division. His technical interests include passive and active remote sensing, radiative transfer theory, electromagnetics, antennas and microwave circuits, electronic instrumentation, meteorology, and oceanography.

Dr. Gasiewski is currently President of the IEEE Geoscience and Remote Sensing Society and was General Chair of the 2nd Combined Optical-Microwave Earth and Atmosphere Sensing Symposium (CO-MEAS 1995). He organized the technical program for the 20th International Geoscience and Remote Sensing Symposium (IGARSS 2000) and is the named General Co-Chair of IGARSS 2006, to be held in Denver, CO. He is a member of the American Meteorological Society, the American Geophysical Union, the International Union of Radio Scientists (URSI), Tau Beta Pi, and Sigma Xi,. He is currently serving as Secretary of USNC/URSI Commission F. He has served on the U.S. National Research Councils Committee on Radio Frequencies (CORF) from 1989 to 1995.

Boba Stankov, photograph and biography not available at the time of publication.

Marian Klein received the M.S. and Ph.D. degrees in electrical engineering from the Technical University (TU) of Kosice, Kosice, Slovak Republic, in 1986 and 1996, respectively.

From 1987 to 1996, he was a Faculty Member within the Faculty of Electrical Engineering and Informatics, TU Kosice. From September 1996 to June 1997, he was a Fulbright Scholar at the Georgia Institute of Technology, Atlanta, working in the Laboratory for Radio Science and Remote Sensing. From June 1997 to August 1998, he was a Guest Worker at the National Oceanic and Atmospheric Administration, Environmental Technology Laboratory, Boulder, CO. Since August 1998, he has been with the Cooperative Institute for Research in Environmental Sciences, University of Colorado, Boulder. The areas of his technical expertise include passive microwave remote sensing and radiative transfer theory.

Dr. Klein is member of the IEEE Geoscience and Remote Sensing Society.

Eni G. Njoku (M'77–SM'83–F'95) received the B.A. degree in natural and electrical sciences from Cambridge University, Cambridge, U.K., in 1972, and the M.S. and Ph.D. degrees in electrical engineering from the Massachusetts Institute of Technology, Cambridge, in 1974 and 1976.

He is currently a Principal Scientist with the Jet Propulsion Laboratory (JPL), Pasadena, CA, and is the JPL Project Scientist for the HYDROS mission. From 1976 to 1977, he was a National Research Council Resident Research Associate. In 1977, he joined JPL. From 1986 to 1990, he served as Discipline Scientist for Ocean and Earth Science Data Systems at NASA Headquarters, Washington, DC, and from 1993 to 1994, he was Manager of the Geology and Planetology Section at JPL. During the 2001–2002 academic year, he was on leave as a Visiting Professor at the Massachusetts Institute of Technology. He is a member of the Aqua Advanced Microwave Scanning Radiometer science team and was Principal Investigator for the IIP OSIRIS technology study. His primary interests are in the use of passive and active microwave remote sensing for hydrology and climate applications. His research involves studies of microwave interactions with land surfaces and retrieval algorithm development.

Dr. Njoku is a member of the American Meteorological Society, the American Geophysical Union, the American Association for the Advancement of Science, Commission F of the International Union of Radio Science, and Sigma Xi. He has served as an Associate Editor of the IEEE Transactions on Geoscience and Remote Sensing (1985–1988) and was the Technical Program Chairman for IGARSS'94 held in Pasadena, CA. He has been a recipient of NASA Group Achievement Awards in 1980, 1982, and 1985, and he was awarded the NASA Exceptional Service Medal in 1985.

David Bosch, photograph and biography not available at the time of publication.

Tommy L. Coleman, photograph and biography not available at the time of publication.

Charles A. Laymon (M'01) received the B.S. degree in geology with honors from St. Lawrence University, Canton, NY, and the Ph.D. degree in geological sciences from the University of Colorado, Boulder, in 1982 and 1988, respectively.

He joined Universities Space Research Association (USRA), Huntsville, AL, in 1991 and is currently a Research Fellow with the USRA Global Hydrology and Climate Center. His research interests include remote sensing of land surface properties and processes, such as soil moisture, vegetation parameters, surface temperature, and energy fluxes, and in the assimilation of these data in hydrologic and climate models for a wide variety of applications.

Dr. Laymon received the Sigma Xi Award in 1982 for excellence in undergraduate research.

Patrick Starks, photograph and biography not available at the time of publication.